Advances in Aircraft and Spacecraft Science, *Vol. 1, No. 3 (2014) 273-289*
DOI: http://dx.doi.org/10.12989/aas.2014.1.3.273

Accuracy and applicable range of a reconstruction technique for hybrid rockets

Harunori Nagata*[1a], Hisahiro Nakayama[2], Mikio Watanabe[2], Masashi Wakita[1] and Tsuyoshi Totani[1]

[1]*Faculty of Engineering, Hokkaido University, Sapporo 060-8628, Japan*
[2]*Graduate School of Engineering, Hokkaido University, Kita 13 Noshi 8, Sapporo 060-8628, Japan*

(Received October 29, 2013, Revised January 27, 2014, Accepted February 5, 2014)

Abstract. Accuracy of a reconstruction technique assuming a constant characteristic exhaust velocity (c^*) efficiency for reducing hybrid rocket firing test data was examined experimentally. To avoid the difficulty arising from a number of complex chemical equilibrium calculations, a simple approximate expression of theoretical c^* as a function of the oxidizer to fuel ratio (ξ) and the chamber pressure was developed. A series of static firing tests with the same test conditions except burning duration revealed that the error in the calculated fuel consumption decreases with increasing firing duration, showing that the error mainly comes from the ignition and shutdown transients. The present reconstruction technique obtains ξ by solving an equation between theoretical and experimental c^* values. A difficulty arises when multiple solutions of ξ exists. In the PMMA-LOX combination, a ξ range of 0.6 to 1.0 corresponds to this case. The definition of c^* efficiency necessary to be used in this reconstruction technique is different from a c^* efficiency obtained by a general method. Because the c^* efficiency obtained by average chamber pressure and ξ includes the c^* loss due to the ξ shift, it can be below unity even when the combustion gas keeps complete mixing and chemical equilibrium during the entire period of a firing. Therefore, the c^* efficiency obtained in the present reconstruction technique is superior to the c^* efficiency obtained by the general method to evaluate the degree of completion of the mixing and chemical reaction in the combustion chamber.

Keywords: hybrid rocket; static firing test; data reduction

1. Introduction

Data reduction from hybrid rocket firings presents unique challenges comparing with other types of chemical rockets. In liquid rocket firings, a feed system supplies liquid propellants into a combustion chamber and propellant flow rates are directly-measurable. In solid rocket firings, the oxidizer to fuel ratio (ξ) is a known value and one can easily calculate the gasification rate of a solid propellant from chamber pressure and nozzle throat area, assuming a constant characteristic exhaust velocity (c^*) efficiency during a firing. A hybrid rocket employs a combination of solid and liquid propellants. Generally, the fuel is the solid side. Although the flow rate of the liquid oxidizer is directly-measurable, it is not for the solid fuel. Because c^* strongly depends on ξ, the

*Corresponding author, Professor, E-mail: nagata@eng.hokudai.ac.jp

http://www.techno-press.org/?journal=aas&subpage=7 ISSN: 2287-528X (Print), 2287-5271 (Online)

direct calculation of the flow rate from chamber pressure and nozzle throat area like a solid rocket case is not possible.

Many traditional data reduction methods in hybrid rocket firings rely on endpoint averaging. Endpoint averaging uses the information of initial and final fuel shapes with the firing duration to determine the average fuel regression rate and the average fuel flow rate. A difficulty comes from the fact that both the regression rate and the fuel flow rate are neither constant during a firing nor linear functions of time. Many combustion experiments have been designed to use short firing durations to minimize this difficulty. However, errors associated with the ignition and shutdown transients can be significant in this case (Frederick Jr. and Greinerf 1996). Another issue to be concerned is that the averaging technique is not unique due to the nonlinear nature of the fuel regression. Different averaging techniques can provide different regression rate laws for the same set of test data as Karabeyoglu *et al*. (2007) pointed out.

Time-resolved measurement of fuel consumption is desirable to minimize uncertainties mentioned above. Previous attempts to measure time-resolved regression of hybrid-fuel grains include measurements with ultrasound (Chiaverini *et al*. 2000, Carmicino and Sorge 2005) and x-ray radiography (Chiaverini *et al*. 2000 and Evans *et al*. 2003). These techniques have the potential to provide time-resolved regression data but require specialized instrumentation. Also, they only provide regression data of one position per one instrument and cannot provide a total fuel consumption rate. Zilwa *et al*. (2004) used acoustic techniques to quantify chamber volume. This method relies on accurately measuring the frequency of the Helmholtz oscillations by a pressure transducer and/or photometric technique. The Helmholtz oscillation frequency is proportional to the inverse of the square root of the chamber volume. A major advantage is that the only instrumentation required for implementing this technique is a high-speed pressure transducer or a photomultiplier tube. However, this method is applicable only to single port hybrid rockets. Olliges *et al*. (2008) developed a diagnostic method using a thrust stand mass balance. They calculated time-accurate mass losses in a hybrid rocket from dynamic coefficients of spring, damping, and mass moment of inertia within 2.5% accuracy. A serious disadvantage of this technique is that it is near-impossible to apply this method to a large scale motor.

Some researchers have developed various reconstruction techniques to obtain fuel consumption rate from measurable data such as chamber pressure and oxidizer flow rate. To our knowledge, Osmon (1966) made the earliest attempt. He developed a method of determining the fuel consumption rate as a function of time from histories of the chamber pressure and the oxidizer flow rate, assuming a constant c^* efficiency. However, the theoretical c^* he used did not include the effect of chamber pressure. Also, he did not indicate how he could determine the averaged experimental c^*. The averaged experimental c^* necessary in this method is different from an experimental c^* widely used, and a complex iterative calculation is necessary to obtain this value. We will discuss this issue in detail in Chapter 5. George *et al*. (2001) employed a similar approach but included the chamber pressure effect in the theoretical c^*. The authors have also used this method (Nagata *et al*. 2006). No specialized equipment is necessary in this method, but it requires a long computation time because a number of complex chemical equilibrium calculations are necessary in two stages of iterative calculations, as we will see in the next chapter. Wernimont and Heister (1999) avoided this difficulty by assuming a constant c^* during firing. However, this assumption is unrealistic because the c^* variation due to the ξ shift during a firing is not an uncommon feature in hybrid rockets. Carmicino and Sorge (2006) eliminated the need for the assumption of a constant c^* efficiency by employing a thrust history as an additional input data.

They showed that the c^* efficiency does not change unless the flow field structure greatly changes. As a result, the assumption of a constant c^* efficiency is reasonable in many cases.

The reconstruction technique assuming a constant c^* efficiency is useful because it requires no special apparatus. Many researchers including us have employed this method. However, the accuracy of the fuel consumption rate obtained by this method is not fully investigated yet. Also, the applicable condition of this method remains unclear. As we will discuss in detail in chapter 5, this method is not applicable when multiple solutions of ξ exists. In this paper, we experimentally investigated the accuracy of the fuel consumption rate obtained by this method. To avoid the difficulty arising from a number of complex chemical equilibrium calculations, we developed a simple approximate expression of theoretical c^* as a function of ξ and the chamber pressure. Also, we clarified the condition under which this reconstruction technique is not applicable. Finally, definitions of theoretical average c^* and experimental c^* efficiency necessary to be used in this reconstruction technique will be discussed.

2. Data reduction method

The following equations give instantaneous values of the total mass flux and the experimental characteristic exhaust velocity

$$\dot{m}_p = \dot{m}_o + \dot{m}_f = \dot{m}_o\left(1+\frac{1}{\xi}\right) \tag{1}$$

$$c^*_{ex} = \frac{p_c A_t}{\dot{m}_p} = \frac{p_c A_t}{\dot{m}_o\left(1+\frac{1}{\xi}\right)} \tag{2}$$

At the same time, a theoretical calculation provides the theoretical characteristic exhaust velocity as a function of ξ and the chamber pressure

$$c^*_{th} = c^*_{th}(\xi, p_c) \tag{3}$$

By introducing the c^* efficiency c^*, we can obtain the following equation

$$\eta c^*_{th}(\xi, p_c) = \frac{p_c A_t}{\dot{m}_o\left(1+\frac{1}{\xi}\right)} \tag{4}$$

in which we assume a constant c^* efficiency η during a firing. Unknown values in the above equation are η and ξ. By assuming a value for η, we can obtain ξ by solving the above equation. After obtaining ξ, the following equation provides the instantaneous value of the fuel flow rate

$$\dot{m}_f = \frac{\dot{m}_o}{\xi} \tag{5}$$

The integral of the above equation gives the total fuel mass consumption during a firing

$$M_f = \int_0^{t_b} \dot{m}_f dt = \int_0^{t_b} \frac{\dot{m}_o}{\xi} dt \tag{6}$$

An iterative calculation is necessary to adjust the value of η so that the calculated total fuel mass consumption agrees with the experimental result.

We used the CEA code to calculate the theoretical c^*, employing "infinite area combustor" model with the frozen-flow assumption (Gordon and McBride 1994). The CEA code determines temperature and chemical composition of a combustion gas through many iterative calculations. Additionally, this reconstruction technique requires two stages of iterative calculations; one for ξ and the other for η. These many iterative calculations lengthen the calculation time. To avoid this problem, we developed an approximate expression of the theoretical characteristic exhaust velocity as a function of ξ and the chamber pressure. The characteristic exhaust velocity (c^*) depends strongly on ξ and weakly on the chamber pressure, as Fig. 1 shows. Because it appears that c^* exhibits an exponential dependence on the chamber pressure, we employed the following equation as the approximate expression

$$c^*_{apx}(\xi, p_c) = c^*_{apx}(\xi, p_{c,low}) + \left[c^*_{apx}(\xi, p_{c,up}) - c^*_{apx}(\xi, p_{c,low})\right] \frac{ln\ p_c - ln\ p_{c,low}}{ln\ p_{c,up} - ln\ p_{c,low}} \tag{7}$$

where $c^*_{apx}(\xi, p_{c,up})$ and $c^*_{apx}(\xi, p_{c,low})$ are approximate equations when the chamber pressures are at an upper limit ($p_{c,up}$) and a lower limit ($p_{c,low}$), respectively. Both approximate equations depend only on ξ. To improve the precision of the approximations, we adopted expressions of degree nine, using the least square method, to five partitions of ξ ranges (0.01 to 0.58, 0.58 to 0.68, 0.68 to 4.0, 4.0 to 50.0, and 50.0 to 100.0) for both approximate equations. Lower and upper limits of the chamber pressure were 0.1 and 10.0 MPa, respectively.

The approximate expression, Eq. (7), shows high accuracy across the wide ranges of ξ and the chamber pressure. To evaluate the accuracy, we calculated the standard deviation (S) of the approximation as a function of chamber pressure (p_c) by the following equation

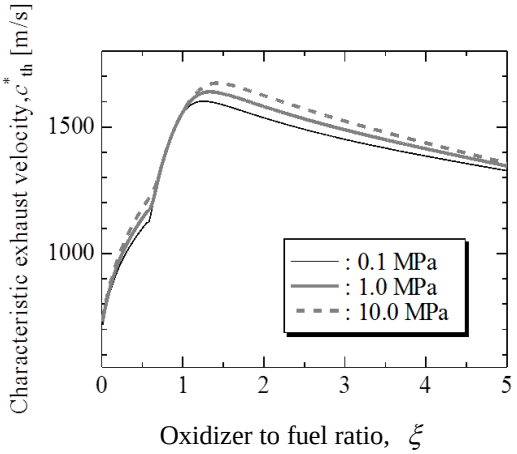

Fig. 1 Theoretical characteristic exhaust velocity (c^*_{th})

$$S(p_c)=\sqrt{\frac{\int_{\xi_1}^{\xi_2}\left[c^*_{th}(\xi,p_c)-c^*_{apx}(\xi,p_c)\right]^2 d\xi}{\xi_2-\xi_1}} \tag{8}$$

in which ξ_1 and ξ_2 are 0.01 and 4.0, respectively. Fig. 2 shows the result. Standard deviations less than 3 m/s are very small comparing with the characteristic exhaust velocities Fig. 1 shows. It appears that the standard deviation reaches its peak at p_c around 1 MPa. That means if the accuracy of Eq. 7 is satisfactory at 1 MPa, the accuracy is acceptable across the pressure range from 0.1 to 10 MPa. Fig. 3 shows the error of the estimation as a function of ξ when the chamber pressure is 1 MPa. The error is less than 1%, showing that the accuracy of the approximate expression, Eq. (7), is acceptable across the wide ranges of ξ and the chamber pressure.

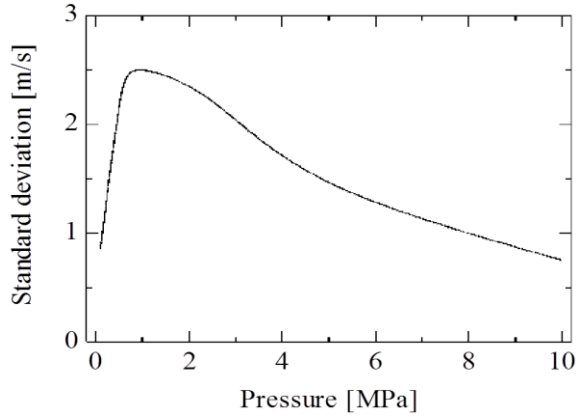

Fig. 2 Standard deviation of the approximation formula (Eq. (7)) as a function of chamber pressure

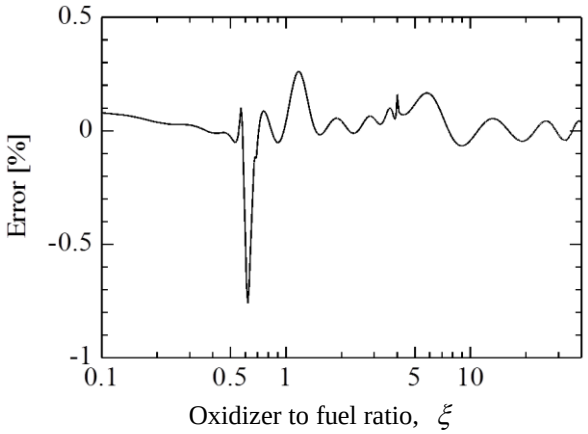

Fig. 3 Error of the approximation formula (Eq. (7)) as a function of ξ. The chamber pressure is 1 MPa

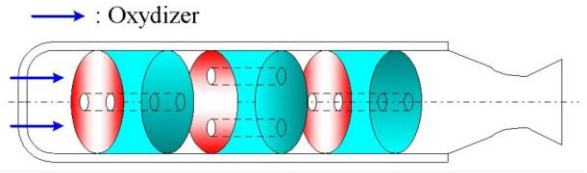

Fig. 4 Schematic view of a CAMUI type hybrid fuel grain

3. Static firing tests

Although a test motor we employed in this research is one of CAMUI type (Nagata *et al*. 1998), the present reconstruction technique is applicable to all types of hybrid motors. The name CAMUI comes from an abbreviation of "cascaded multistage impinging-jet" representing the new fuel grain design Fig. 4 shows. By changing a conventional cylinder-shape solid fuel with a central port into multiple stages of cylinder blocks, end faces of all blocks burn concurrently. The grain design makes the combustion gas collide repeatedly with fuel surfaces, resulting in intense heat transfer to the fuel. Fig. 5 shows the detail of a test motor. It consists of an injector, an igniter, a water-cooled combustion chamber and a convergent nozzle, and a diffuser. Liquid oxygen (LOX) flows into the combustion chamber through a pair of injectors Fig. 6 shows. Each injector has blocks and fuel spacers made of poly-methyl-methacrylate (PMMA). Fig. 7 shows the geometry of a fuel block and a fuel grain. The outer diameter and the axial length of a fuel block are 70 mm and 50 mm, respectively. Each fuel block has two axial ports of 10 mm in diameter at axially opposite locations with each other. The distance between the two ports is 35 mm, the same three ejection holes of 0.5 or 0.7 mm in diameters. A fuel grain consists of three cylindrical fuel distance between the two injectors. Adjoining injectors or ports are in 90-degree staggered orientation with each other to make the combustion gas or oxidizer streams collide repeatedly with

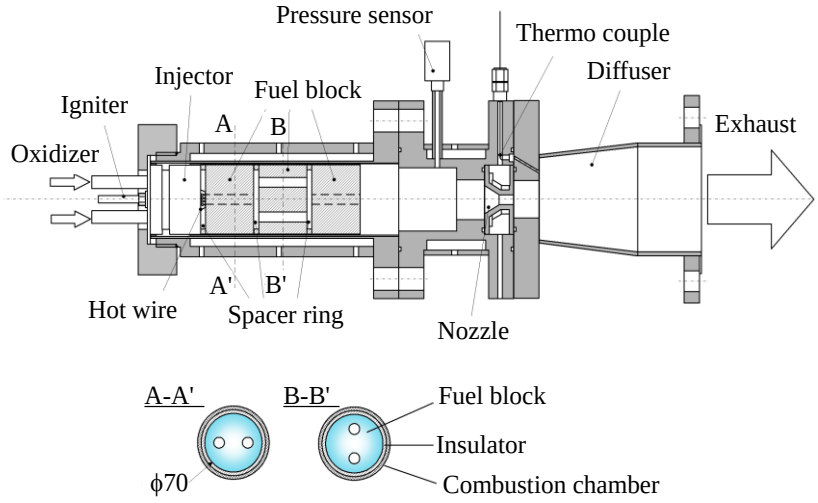

Fig. 5 Schematic view of the test motor

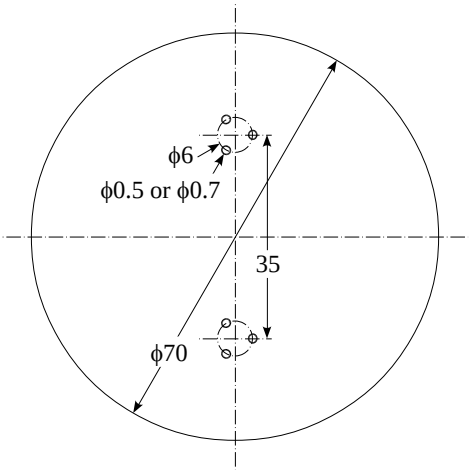

Fig. 6 Injectors in the test motor

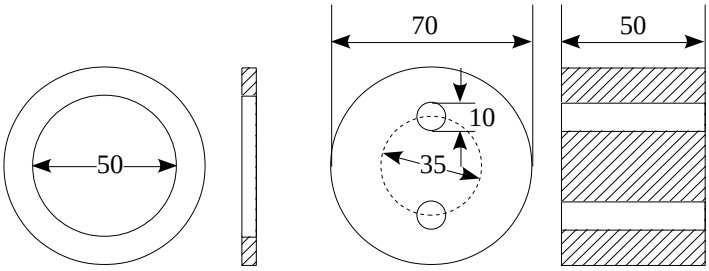

Fig. 7 Injectors in the test motor

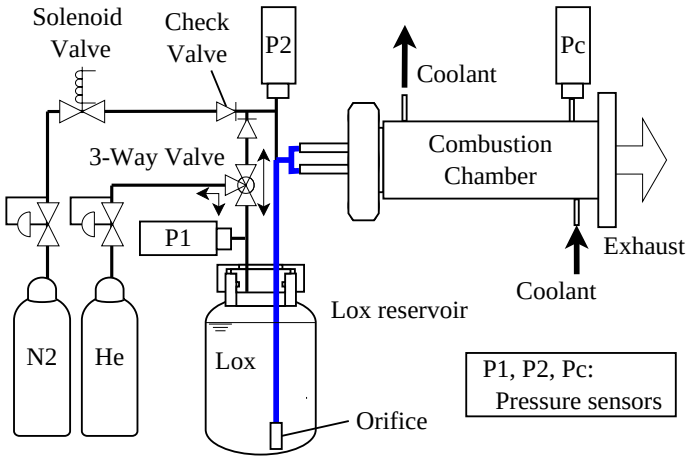

Fig. 8 Experimental apparatus

Table 1 Test conditions

Test index	LOX flow rate* [g/s]	Initial fuel weight [g]	Final fuel weight [g]	Fuel consumption [g]	Chamber pressure* [MPa]	Burning duration [s]
01	52	683	245	438	0.94	10.5
02	25	683	515	168	0.40	5.5
03	27	683	366	317	0.48	10.6
04	28	683	247	435	0.50	15.8
05	35	683	323	360	0.63	9.8
06	22	683	443	240	0.27	9.4
07	34	683	332	351	0.58	10.1
08	36	683	323	360	0.65	9.9
09	28	683	349	334	0.50	10.4
10	45	683	269	414	0.85	10.3
11	59	683	215	468	1.08	10.4

*Average value during a firing test

fuel surfaces. Spacer rings with the outer diameter of 70 mm, being the same with that of a fuel block, keep the flow path of combustion gas between blocks. The axial length of spacers decides the initial block spacing to be 5 mm. The inner diameter of the water-cooled convergent nozzle is 13.5 mm.

Fig. 8 shows the outline of the experimental apparatus. It mainly consists of a pressurization device using helium, a LOX reservoir, and the test motor. The inner volume of the LOX reservoir is 1.0 L. Heat insulating materials wraps LOX lines. These lines were cooled enough before each test. As a noteworthy feature in the LOX feeding system, there is no valve in the liquid oxygen line. Before starting liquid oxygen feeding, evaporating oxygen gas (GOX) outflows from the tank to the motor through the 3-way valve. This evacuation serves two purposes: One is to avoid self-pressurization of the liquid oxygen. The other is to help ignition of an igniter fuel on the upstream end face of the uppermost fuel block. A nichrome wire ignites the igniter fuel by electrical heating. Ignition is easily detectable by viewing smoke out of the exhaust nozzle. A few seconds after ignition, the 3-way valve opens the line for applying pressure to the LOX reservoir and closes the GOX line simultaneously to start feeding LOX into the combustion chamber. After a prescribed firing duration, a valve relieves the pressure of the LOX reservoir to stop the feeding. Simultaneously, nitrogen gas purges the combustion chamber to stop firing quickly. Main measurement items during a firing were combustion chamber pressure and LOX flow rate. A differential pressure type flow meter in the LOX reservoir measures LOX flow rate. After each firing test, residual fuel grain was recovered from the combustion chamber to measure the fuel consumption.

Table 1 summarizes test conditions. From 02 to 04 were in the same test conditions except burning durations to examine a fuel consumption history. From 05 to 11 were to find out the effect of LOX flow rate under almost the same firing durations.

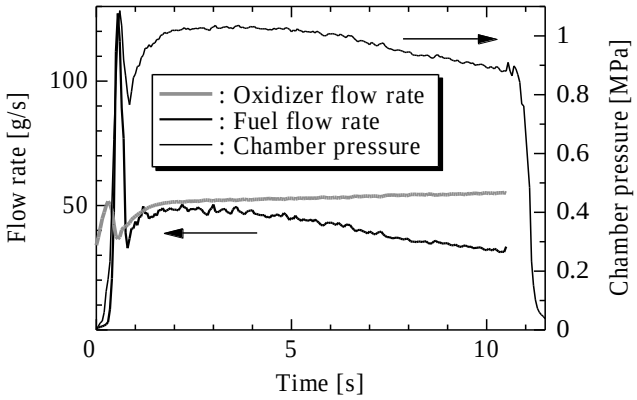

Fig. 9 Histories of propellant flow rates and chamber pressure

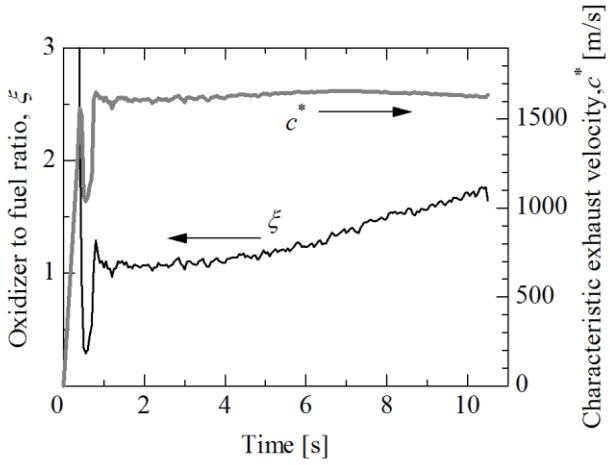

Fig. 10 Histories of c^* and ξ

4. Results

Fig. 9 shows results of test-01 as an example of calculated fuel flow history together with histories of chamber pressure and LOX flow rate, which are measurable quantities. The initial pressure spike is due to a rapid reaction between fuel-rich combustion gas and oxygen. Because the fuel ignites with low-flux oxygen supplied by the LOX gasification, the combustion chamber is filled with fuel-rich combustion gas when the LOX starts flowing into the chamber. As the result of this initial rapid reaction, the calculated fuel flow rate shows an unrealistic rapid increase initially. This unreal rapid increase can cause 2% to 3% overestimation of total fuel consumption. The motor start time was defined as the moment of the initial pressure rise being greater than the fluctuation amplitudes of the signal. After steady combustion, the chamber pressure sharply falls down due to the stop of LOX supply. We employed the bisector method (Sutton and Biblarz 2000) to determine motor stop time. This approach uses two lines running along the last

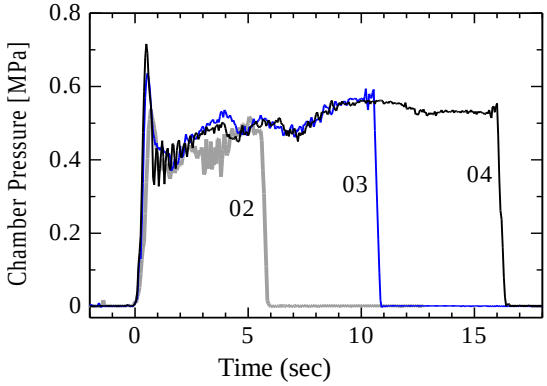

Fig. 11 Chamber pressure histories

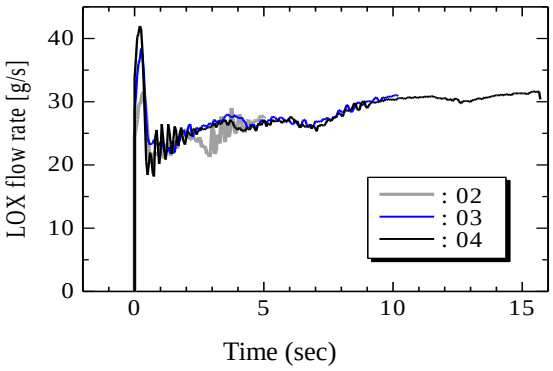

Fig. 12 LOX flow rate histories

Table 2 Results of the firing tests

Test no.	Time [s]	Test results		Calculated		Error
		Fuel weight [g]	Consumption [g]	Fuel weight [g]	Consumption [g]	
-	0	683	0	683	0	-
02	5.05	515	168	534	148	0.116
03	10.2	366	317	382	300	0.051
04	15.7	247	435	247	435	-

portion of the steady-state burn and the initial portion of the tail-off. The time location at which these two lines intersect is the stop time.

Fuel flow rate decreases with time because forward-end face areas of fuel blocks, which are main burning surfaces in this fuel design, decrease with the expansion of port diameters. As a result, ξ increases with time as Fig. 10 shows. Calculated c^* efficiency (η) was 1.01. Considering a possible error of around 3% due to the overestimation of the fuel flow rate at the startup and the theoretical c^* approximation, the actual value of η may be 0.98 or higher. The calculated fuel flow rate history agrees with the one we can expect from the regression progress of fuel blocks.

To examine the accuracy of the present reconstruction technique, we conducted a series of static firing tests with the same test conditions except burning durations (02, 03, and 04). Figs. 11 and 12 show histories of chamber pressures and LOX flow rates, respectively. These results show that the reproducibility of these firing tests was acceptable. Fig. 13 shows a reconstructed fuel weight history together with experimental residual fuel weights. The solid line in the figure is the fuel weight history calculated from the data of test-04. Open circles mark firing durations and fuel weights after firing tests. The test results of 02 and 03 lie near the solid line, showing accuracy of the present data reduction method. Table 2 summarizes the results. Experimental and calculated fuel consumptions at 5.05 s were 168 g and 148 g, respectively, which resulted in an error of 11.6%. This error decreased to 5.1% with firing duration going up to 10.2 s. Note that the differences between the calculated and measured values are close with each other; 20 g at 5.05 s and 17 g at 10.2 s. Because the error mainly comes from the ignition and shutdown transients, error tends to decrease with increasing firing duration.

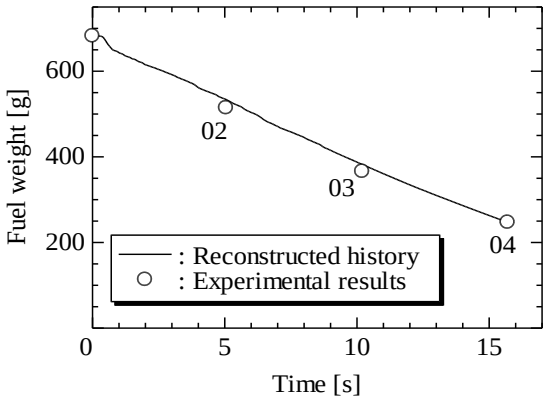

Fig. 13 Reconstructed fuel weight history together with experimental residual fuel weights

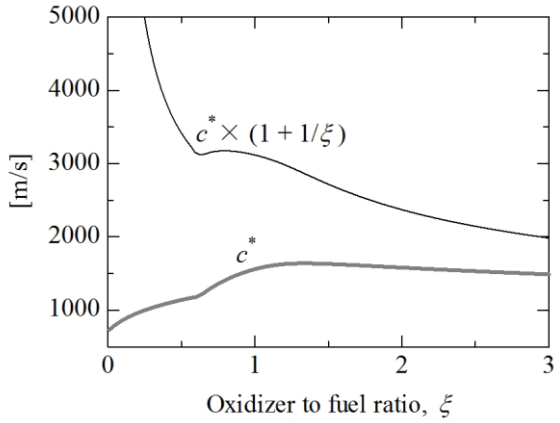

Fig. 14 Variations of c^* (theoretical) and $c^*\left(1+\frac{1}{\xi}\right)$ depending on ξ. The chamber pressure is 1 MPa

5. Discussions

Because the present reconstruction technique calculates the fuel flow rate by solving Eq. 4, we encounter a difficulty when Eq. (4) has multiple solutions. To clarify the range of ξ in which this difficulty occurs, we rearrange Eq. (4) as follows

$$\eta c_{th}^*(\xi, p_c)\left(1+\frac{1}{\xi}\right) = \frac{p_c A_t}{\dot{m}_o} \tag{9}$$

Fig. 14 shows the left hand side of Eq. (9) when the c^* efficiency η is unity, together with the theoretical c^*. This figure shows a range of ξ, from 0.6 to 1.0, in which this function has multiple ξ to give a single output value. Fig. 15 shows an enlarged view. Accordingly, Eqs. (4) and (9) have multiple solutions in this range. Fig. 16 shows an example of this difficulty. Solid and broken lines are variations of theoretical and numerical c^* depending on ξ when a solution of ξ is 0.7.

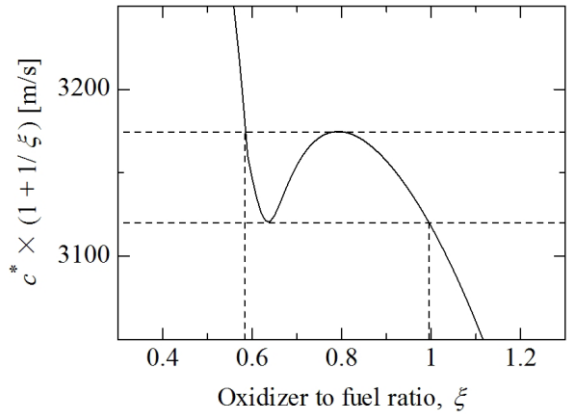

Fig. 15 Variation of $c^*\left(1+\frac{1}{\xi}\right)$ as a function of ξ around the range of multiple solutions

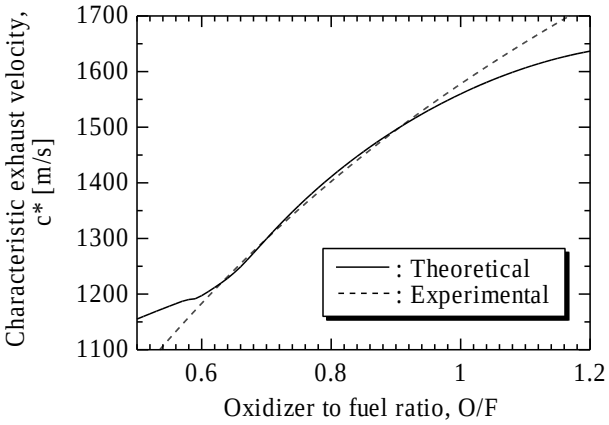

Fig. 16 Theoretical and experimental c^* depending on *O*/*F* as an example encountering the difficulty of multiple solutions

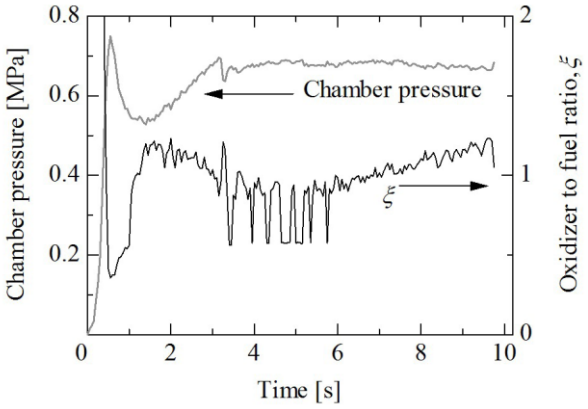

Fig. 17 A fluctuating ξ history as an example encountering the difficulty of multiple solutions

Besides the supposed solution ($\xi = 0.7$), these two lines intersect at other two points ($\xi = 0.64$ and 0.9). Another difficulty is that a small variation of the chamber pressure causes a large variation of the solution. Only 1% of a pressure overestimation (or an underestimation) moves the solution of ξ to 0.6 (or 0.98). Fig. 17 shows histories of chamber pressure and calculated ξ obtained by the test-05, showing an example encountering this difficulty. Mean flow rates of LOX and fuel were 35 g/s and 36.7 g/s, respectively. The mean ξ of 0.95 is in the multiple solution range. As a result, the ξ history shows a large fluctuation ranging from 0.6 to 0.9 during 3.5 s to 6 s.

Note that the c^* efficiency defined by Eq. 4 is different from an experimental c^* efficiency obtained by a general method. For simplicity, we assume a constant nozzle throat area A_t during a burning period in the following discussion. As an instantaneous value, the following equation gives an experimental c

$$c_{ex}^* = \frac{p_c A_t}{\dot{m}_f + \dot{m}_o} \tag{10}$$

Generally, the following equation gives an experimental c^* and an average c^* efficiency

$$\bar{c}_{ex}^* \equiv \frac{\bar{p}_c A_t}{\bar{\dot{m}}} = \eta_{ex} c_{th}^* \left(\bar{\xi}_{ex}, p_c \right) \equiv \eta_{ex} \bar{c}_{th,av}^* \tag{11}$$

where

$$\bar{p}_c = \frac{\int_0^{t_b} p_c \, dt}{t_b} \tag{12}$$

$$\bar{\dot{m}}_p = \frac{\int_0^{t_b} \left(\dot{m}_f + \dot{m}_o \right) dt}{t_b} \tag{13}$$

$$\bar{\xi} = \frac{\int_0^{t_b} \dot{m}_o \, dt}{\int_0^{t_b} \dot{m}_f \, dt} \tag{14}$$

and $\bar{c}_{th,av}^*$ is theoretical c^* at the average values ($\bar{\xi}_{ex}$ and $\bar{p}_c$). As we will show in the following discussion, η_{ex} does not usually agree with η defined by Eq. (4). From Eq. (4), the following equation gives the chamber pressure p_c

$$p_c = \frac{\eta c_{th}^* \dot{m}_o \left(1 + \frac{1}{\xi} \right)}{A_t} = \frac{\eta c_{th}^* \left(\dot{m}_f + \dot{m}_o \right)}{A_t} \tag{15}$$

By substituting the above equation into Eq. (12), we get an experimental c^* and c^* efficiency again. Note that this time the c^* efficiency is a mass-averaged value

$$\frac{\bar{p}_c A_t}{\dot{\bar{m}}} = \bar{c}^*_{ex} = \frac{\eta \int_0^{t_b} c^*_{th}\left(\dot{m}_f + \dot{m}_o\right) dt}{\int_0^{t_b} \left(\dot{m}_f + \dot{m}_o\right) dt} = \eta \bar{c}^*_{th,\,mass} \tag{16}$$

where $\bar{c}^*_{th,\,mass}$ is a mass-averaged theoretical c^* efficiency, given by the following equation

$$\bar{c}^*_{th,\,mass} = \frac{\int_0^{t_b} c^*_{th}\left(\dot{m}_f + \dot{m}_o\right) dt}{\int_0^{t_b} \left(\dot{m}_f + \dot{m}_o\right) dt} \tag{17}$$

Because c^* is a strong function of ξ, theoretical c^* at the average values and c^* efficiency obtained by Eq. (11) do not agree with the mass-averaged theoretical values when ξ is not constant during a firing. When the average ξ given by Eq. (14) is near the optimal value, $\bar{c}^*_{th}$ likely exceeds $\bar{c}^*_{th,\,mass}$ because $\bar{c}^*_{th}$ does not take c^* loss due to the ξ shift during a firing into account. Osmon mentioned in his paper (Osmon 1966) that the c^* efficiency is equal to that calculated from the average theoretical and experimental c^*. However, he did not indicate how he determined the average values. If he determined the average theoretical c^* by Eq. 11, the total fuel mass consumption calculated by Eq. (6) would not agree with the experimental value. An iterative calculation is necessary to obtain the average value by Eq. (16) because the fuel flow rate history is necessary to calculate the average value. However, he did not mention any iterative calculation to obtain this average value at all. It is noteworthy that because of this, $\eta_{ex,time}$ can be below unity even when the combustion gas keeps complete mixing and chemical equilibrium during the entire period of a firing. In contrast, η defined by Eq. 4 becomes unity in this case. Therefore, η is superior to $\eta_{ex,time}$ to evaluate the degree of completion of the mixing and chemical reaction in the combustion chamber.

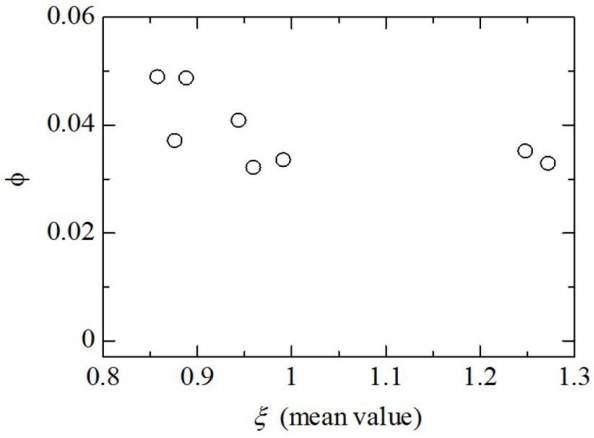

Fig. 18 Variation of the average c^* deviation ϕ when the firing duration is around 10 seconds

Now we define average c^* deviation ϕ by the following equation

$$\phi = \frac{\overline{c}^*_{th,av}}{\overline{c}^*_{th,mass}} - 1 \tag{18}$$

Fig. 18 shows the variation of the average c^* deviation ϕ when the firing duration is around 10 seconds (test 01, 03, and 05 to 11), with the horizontal axis of the average ξ defined by Eq. 14. The discrepancies were around 3% to 5% and tend to increase when ξ goes through a region where c^* is sensitive to ξ.

6. Conclusions

Accuracy of a reconstruction technique assuming a constant c^* efficiency for reducing hybrid rocket firing test data was examined experimentally. To avoid the difficulty arising from a number of complex chemical equilibrium calculations, we developed a simple approximate expression of theoretical c^* as a function of ξ and the chamber pressure. The error of the approximate expression was less than 1% across the wide ranges of ξ (0.01 to 100) and chamber pressure (0.1 to 10 MPa). A series of static firing tests with the same test conditions except burning durations revealed that the error in the calculated fuel consumption decreases with increasing firing duration. This is because the error mainly comes from the ignition and shutdown transients.

The present reconstruction technique obtains ξ by solving an equation between theoretical and experimental c^* values. Therefore, we encounter a difficulty when multiples solutions of ξ exists. In the PMMA-LOX combination, a ξ range of 0.6 to 1.0 corresponds to this case.

Definition of c^* efficiency necessary to be used in this reconstruction technique is different from a c^* efficiency obtained by a general method. Generally, c^* efficiency is an average c^* divided by a theoretical value at an average ξ and chamber pressure. Because the average c^* includes the c^* loss due to the ξ shift, this c^* efficiency can be below unity even when the combustion gas keeps complete mixing and chemical equilibrium during the entire period of a firing. Therefore, the c^* efficiency obtained in the present reconstruction technique is superior to the c^* efficiency obtained by the general method to evaluate the degree of completion of the mixing and chemical reaction in the combustion chamber.

Acknowledgements

This research is supported by the Ministry of Education, Science, Sports and Culture, Grant-in-Aid for Scientific Research (A), 40281787, 2012. This research is supported by the Hybrid Rocket Research Working Group (HRrWG) of Institute of Space and Astronautical Science, Japan Aerospace Exploration Agency. The authors thank members of HRrWG for their helpful discussion.

References

Carmicino, C. and Sorge, A.R. (2005), "Role of injection in hybrid rockets regression rate behavior", *J.*

Propul. Power, **21**(4), 606-612.
Carmicino, C and Sorge, A.R. (2006), "Influence of a conical axial injector on hybrid rocket performance", *J. Propul. Power*, **22**(5), 984-995.
Chiaverini, M.J., Serin, N., Johnson, D.K., Lu, Y.C., Kuo, K.K. and Risha, G.A. (2000), "Regression rate behavior of hybrid rocket solid fuels", *J. Propul. Power*, **16**(1), 125-132.
Evans, B., Risha, G.A., Favorito, N., Boyer, E., Wehrman, R., Libis, N. and Kuo, K.K. (2003), "Instantaneous regression rate determination of a cylindrical x-Ray transparent hybrid rocket motor", *39th AIAA/ASME/SAE/ASEE Joint Propulsion Conference and Exhibit*, AIAA 2003-4592.
Frederick Jr., R.A. and Greiner, B.E. (1996), "Laboratory-scale hybrid rocket motor uncertainty analysis", *J. Propul. Power*, **12**(3), 605-611.
George, P., Krishnan, S., Varkey, P.M., Ravindran, M. and Ramachandran, L. (2001), "Fuel regression rate in hydroxyl-terminated-polybutadiene/gaseous-oxygen hybrid rocket motors", *J. Propul. Power*, **17**(1), 35-42.
Gordon, S. and McBride, B.J. (1994), "Computer program for calculation of complex chemical equilibrium compositions and applications", *NASA Reference Publication*, RP-1311.
Karabeyoglu, M.A., Cantwell, B.J. and Zilliac, G. (2007), "Development of scalable space–time averaged regression rate expressions for hybrid rockets", *J. Propul. Power*, **23**(4), 737-747.
Nagata, H., Okada, K., Sanda, T., Akiba, R., Satori, S. and Kudo, I (1998), "New fuel configurations for advanced hybrid rockets", *49th International Astronautical Congress*, IAF-98-S.3.09
Nagata, H., Ito, M., Maeda, T., Watanabe, M., Uematsu, T., Totani, T. and Kudo, I. (2006), "Development of CAMUI hybrid rocket to create a market for small rocket experiments", *Acta. Astronautica*, **59**(1-5), 253-258.
Olliges, J.D., Lilly, T.C., Joslyn, T.B. and Ketsdever, A.D. (2008), "Time accurate mass flow measurements of solid-fueled systems", *Rev. Sci. Instrum.*, **79**, 101301.
Osmon, R.V. (1966), "An Experimental Investigation of a Lithium Aluminum Hydride-Hydrogen Peroxide Hybrid Rocket", *J. Aerospace Eng.*, **62**(61), 92-102.
Sutton, G.P. and Biblarz, O. (2000), *Rocket Propulsion Elements* (7th Edition), John Wiley & Sons, Inc., New York, NY, USA.
Wernimont, E.J. and Heister, S.D. (1999), "A reconstruction technique for reducing hybrid rocket combustion test data", *J. Propul. Power*, **15**(1), 128-136.
Zilwa, S.D., Zilliac, G., Reinath, M. and Karabeyoglu, M.A. (2004), "Time-resolved fuel-grain port diameter measurement in hybrid rockets", *J. Propul. Power*, **20**(4), 684-689.

EC

Nomenclature

A_t	=	nozzle throat area
c^*	=	characteristic exhaust velocity
c^*_{apx}	=	approximate value of characteristic exhaust velocity obtained by Eq. (7)
c^*_{ex}	=	experimental characteristic exhaust velocity obtained by Eq. (2)
c^*_{th}	=	theoretical characteristic exhaust velocity
$\bar{c}^*_{ex}$	=	averaged experimental characteristic exhaust velocity obtained by Eq. (11).
$\bar{c}^*_{th,mass}$	=	mass-averaged theoretical characteristic exhaust velocity
$\bar{c}^*_{th,av}$	=	theoretical characteristic exhaust velocity at averaged values (see Eq. (11)).
$\dot{m}_f$	=	instantaneous fuel mass flow rate (a function of time)
$\dot{m}_o$	=	instantaneous oxidizer mass flow rate (a function of time)
$\dot{m}_p$	=	instantaneous propellant mass flow rate (a function of time)
$\overline{\dot{m}}_p$	=	time-averaged propellant mass flow rate
M_f	=	total fuel mass consumption obtained by Eq. (6)
p_c	=	instantaneous combustion chamber pressure (a function of time)
$\bar{p}_c$	=	time-averaged combustion chamber pressure
$p_{c,low}$	=	lower limit of the combustion chamber pressure used in Eq. (7)
$p_{c,up}$	=	upper limit of the combustion chamber pressure used in Eq. (7)
S	=	Standard deviation defined by Eq. (8)
t_b	=	burning duration
ϕ	=	average c^* deviation defined by Eq. (17)
η	=	c^* efficiency defined by Eq. (4)
η_{ex}	=	c^* efficiency defined by Eq. (10)
ξ	=	oxidizer to fuel ratio
$\bar{\xi}$	=	time-averaged oxidizer to fuel ratio